Experimental study of an attitude estimator with measurement disturbance rejection

Gustav Öman Lundin, Philippe Mouyon, and Augustin Manecy

Abstract Attitude estimation is a corner stone of the flight stability or safety for UAVs. Even if a large panorama of efficient solutions exists, it is still difficult to guarantee the accuracy of the attitude filter during common disturbances (large accelerations or local magnetic disturbances). The integrity of the covariance (accuracy estimation) is also a difficult point in both nominal and disturbed case. This paper introduces a fault tolerant architecture for attitude estimation. It is intended to handle sensor malfunctions and unexpected environmental disturbances. The estimation architecture consists of three distinctive parts: a set of sensor models to detect incoherent or corrupted sensor measurements; a sensor data health check which activates or deactivates the state correction of the attitude filter; an attitude filter including a saturated gyroscope bias model and a decoupling between the roll/pitch and yaw angles. Simulation and experimental results show that the proposed architecture handles both inertial acceleration disturbances and magnetic disturbances without the need for speed or position measurements, or drag force models.

1 Introduction

An accurate and robust attitude estimation is crucial in GNC-applications. The attitude calculation lies at the core of GNC systems and therefore directly impacts the system stability. In addition, the attitude estimate must remain integrate, meaning that the actual attitude should lie within a certain confidence interval of the estimated attitude.

Gustav Öman Lundin
ONERA, F-31055 Toulouse, France, e-mail: gustav.oman_lundin@onera.fr

Philippe Mouyon
ONERA, F-31055 Toulouse, France, e-mail: philippe.mouyon@onera.fr

Augustin Manecy
ONERA, F-31055 Toulouse, France, e-mail: augustin.manecy@onera.fr

The accuracy of the attitude estimation will naturally depend on the quality of the sensors involved and its robustness on the redundancy (physical or analytical), and the numerical stability of the algorithm used to fuse the sensor data.

In low-cost/low-weight applications, MEMS-sensors for gyroscope, accelerometer, and magnetometer measurements are the usual go-to. The main issue of these sensors is apart from their low accuracy, that the are easily disturbed. The gyroscope being the most reliable sensor in terms of accuracy, will be subject to bias and scale factors. Accelerometers are disturbed by inertial accelerations and vibration. Magnetometers will only work well in environments free from magnetic disturbances.

A way of handling this problem is to use a force model to reconstruct the sensor data ([1], [2]), although this requires precise knowledge of the vehicle properties and it may couple the actuator and sensor failure detection. Alternatively one can make use of auxiliary sensors such as a GNSS receivers ([3], [4], [5]). But this requires good refresh rates and good conditions (clear-sky) to be efficient and it is not reliable close to the ground, buildings or trees due to multi-trajectory. This will also create the need for failure detection of the auxiliary sensors (e.g., jump in GNSS solution).

Yet another solution, is the use of performance models that model the behaviour of the sensor itself. The standard attitude estimation assumptions are zero specific acceleration and a locally known magnetic field, see for example [6]. In [7] the local magnetic field is supposed to be regular enough that its evolution can be tracked by measuring its gradient. An alternative presented herein is to assume that the sensors will indicate their inertial references (e.g. gravity) in finite time.

In regards to reliable attitude filters, many recent works concern either complementary filters [8] with guaranteed convergence or various Kalman filters ([9], [10], [11]). In an attempt to bridge the gap, [12] recently proposed a cascaded nonlinear osbserver coupled with a Kalman filter. In [13], a filter based on the evolution of body vector measurements is introduced. In practical implementations, both types have shown good results. Whilst the complementary filter will always get you home, the notion of covariance of the Kalman filter will indicate roughly how lost you are on your way (although a Kalman filter did get man to the moon and back [14]).

To improve the robustness of an attitude filter, one can decouple the yaw estimation from the inclination (roll/pitch) estimation by mixing the accelerometer and magnetometer measurements [15]. The obvious weakness of this approach is that potential accelerometer faults will impact the yaw estimation directly.

In this paper we propose an architecture that uses performance models coupled with a set of statistical tests to detect sensor anomalies, in order to not use corrupted sensors' measurements. The attitude is then estimated by a nonlinear Kalman Filter (NLKF) using a modified correction step. Instead of correcting the entire attitude in one go, our filter uses a sequential correction to update the inclination and heading separately by imposing a structured correction.

The robustness of the attitude estimation is further improved by introducing a saturated bias model similar to [16] which limits the growth of the gyroscope bias in case of erroneous measurements or prolonged periods without state corrections. The problem of properly linearising such a model is further treated in order to get a correct estimation of the associated covariance. The estimation architecture is finally

validated by confronting the ground truth (measured by a motion capture system) to the estimation results obtained during flight tests with a quadrotor UAV. The estimations of the proposed architecture are also compared tot he well known filter of the Pixhawk solution, during nominal flight, but also in case of high acceleration and magnetic disturbances.

Paper structure

The paper begins with an introduction of the attitude estimation problem in section 2 and the general extended Kalman filter (EKF) equations in section 3. An overview of the fault tolerant estimation architecture is given in section 4 along with tuning considerations in section 5. Experimental results are presented in section 6 for three typical trajectories with and without magnetic disturbances. Some conclusions on the effectiveness of the architecture with regards to large accelerations and magnetic disturbances are finally drawn in section 7.

2 The attitude estimation problem

The rotation of the body fixed frame (B) w.r.t the inertial frame (I) is given by the rotational matrix R. We define the rotation direction from the body frame to inertial frame by R, and the inverse rotation by $R^{-1} = R^T$, i.e:

$$\mathbf{r}_B = R^T \mathbf{r}_I \quad \Leftrightarrow \quad \mathbf{r}_I = R\,\mathbf{r}_B \tag{1}$$

The attitude estimation problem consists of finding vector measurements $\mathbf{r}_{B,m}$ satisfying (1) for some vector $\mathbf{r}_{I,ref}$. A rotation can be more conveniently expressed with a unit vector η and an angle β, i.e. a *unit quaternion* defined as

$$\mathbf{q} \triangleq (\cos(\beta/2)\,,\, \eta\,\sin(\beta/2))^T = (s, \mathbf{n})^T\,. \tag{2}$$

The relation between R and $\mathbf{q}$ is called Rodrigues' formula and is written as $R(\mathbf{q}) \triangleq I - 2s\,\mathbf{v}_\times + 2\mathbf{v}_\times^2$, where $\mathbf{v}_\times$ is the skew-symmetric representation of $\mathbf{v}$. The quaternion kinematics are given by

$$\dot{\mathbf{q}} = \frac{1}{2}\Omega(\omega)\mathbf{q}, \quad \Omega(\omega) = \begin{bmatrix} 0 & -\omega^T \\ \omega & \omega_\times \end{bmatrix}\,, \tag{3}$$

where $\omega \triangleq (\omega_x, \omega_y, \omega_z)^T$ is the vector of body angular rates. For the passage to discrete time, Euler's method can be used if the integration is small enough, however it produces a quaternion which is no longer unitary and must be normalised:

$$\begin{aligned} \tilde{\mathbf{q}}_{k+1} &= \mathbf{q}_k + \frac{1}{2}\Omega(\omega)\,\Delta t\,\mathbf{q}_k \\ \mathbf{q}_{k+1} &= \frac{\tilde{\mathbf{q}}_{k+1}}{||\tilde{\mathbf{q}}_{k+1}||} \quad \text{(Normalisation)} \end{aligned} \tag{4}$$

In MEMS applications, factors such as sensor noise have a much larger impact when the integration step is small, than this normalisation step.

3 The Kalman filter

As seen above, attitude estimation is a nonlinear estimation problem, we therefore require a nonlinear filtering method. In this work, it was chosen to use mainly the Extended Kalman Filter (EKF), as it allow to both estimate state and associated covariance, i.e., uncertainty. The proposed architecture uses three different filters, two EKF for the sensor performance models, and one NLKF (nonlinear Kalman Filter) as the main attitude estimator. The use of an NLKF instead of a classical EKF is due to the correction method used for the quaternion to keep the quaternion's physical meaning and decouple the inclination and heading dynamics (more details are given in section 4.3.2)

3.1 The Kalman machinery

Given the non-linear model:

$$\begin{aligned} \mathbf{x}_{k+1} &= \mathbf{f}(\mathbf{x}_k, \mathbf{u}_k, \mathbf{v}_k) \\ \mathbf{y}_{k+1} &= \mathbf{h}(\mathbf{x}_{k+1}, \mathbf{w}_{k+1}) \end{aligned} \tag{5}$$

where $\mathbf{v}_k \sim \mathcal{N}(\mathbf{0}, V_k)$ and $\mathbf{w}_{k+1} \sim \mathcal{N}(\mathbf{0}, W_{k+1})$ are respectively input and measurement noise. An EKF that provides an estimate $\hat{\mathbf{x}}$ of $\mathbf{x}$ is defined by the following equations (Joseph's form):

$$\begin{array}{ll} \textit{Prediction} & \textit{Correction} \\ \hat{\mathbf{x}}^+_{k+1} = \mathbf{f}(\hat{\mathbf{x}}_k, \mathbf{u}_k) & \hat{\mathbf{x}}_{k+1} = \hat{\mathbf{x}}^+_{k+1} + K_{k+1}\,\nu_{t+1} \\ P^+_{k+1} = F_k P_k F_k^T + G_k V_k G_k^T & P_{k+1} = [I - K_{k+1} H_{k+1}]\,P^+_{k+1}\,[I - K_{k+1} H_{k+1}]^T \\ & \quad + K_{k+1} W_{k+1} K_{k+1}^T \end{array} \tag{6}$$

P denotes the covariance of $\hat{\mathbf{x}}$, ν the innovation, and K the correction gain. The Kalman gain is the value of K which minimizes the covariance, and is given by:

$$\begin{aligned} \nu_{k+1} &= \mathbf{y}_{k+1} - h\left(\hat{\mathbf{x}}^{+}_{k+1}\right) \\ S_{k+1} &= H_{k+1} P^{+}_{t+1} H^{T}_{k+1} + W_{k+1} \\ K_{k+1} &= P^{+}_{k+1} H^{T}_{k+1} S^{-1}_{k+1} \end{aligned} \tag{7}$$

where S is the innovation covariance. The Jacobians F_k, G_k, and H_{k+1} are calculated as

$$F_k = \frac{\partial \mathbf{f}}{\partial \mathbf{x}_k}_{|\hat{\mathbf{x}}_k, \mathbf{u}_k}, G_k = \frac{\partial \mathbf{f}}{\partial \mathbf{v}_k}_{|\hat{\mathbf{x}}_k, \mathbf{u}_k}, H_{k+1} = \frac{\partial \mathbf{h}}{\partial \mathbf{x}_k}_{|\hat{\mathbf{x}}^{+}_{k+1}}. \tag{8}$$

4 New fault tolerant architecture

In this work, we are interested by the convergence of the estimation filter but also (and mainly) by the integrity of the estimated state's covariance, even when temporary disturbances appear on the measurements. This integrity can be achieved thanks to the two following principles:

- *Orthogonal Measurements:* The estimator is built to decouple the inclination and heading estimations, and to make the inclination estimation robust to magnetometer failures and the heading estimation robust to accelerometer failures. This is achieved by not using accelerometer and magnetometer measurements directly, but pseudo-measurements based on them,
- *Fault tolerant mechanisms:* Some mechanisms were introduced to detect invalid measurements, in order to reject or correct them before the correction step. This allows to maintain the integrity of the estimated state and covariance during temporary disturbances on accelerometers and magnetometers.

We propose a new fault tolerant attitude estimator architecture consisting of three distinct stages. The first stage estimates the accelerometer and magnetometer outputs and incorporates a step of statistical testing to detect erroneous measurements (performance models). The second stage aims to consolidate the sensor data, that is to decide whether the estimated output or the actual measurement should be used. The third stage is the actual attitude filter which provides an estimate of the attitude and the gyroscope bias, using virtual inclination and heading measurements based on consolidated accelerometer and magnetometer measurements. An overview of the architecture is seen in Fig. 1.

4.1 Sensor model blocks: "EKF Mag." and "EKF Acc."

These blocks provide an estimate of the sensor outputs using an EKF. We denote the sensor output estimation by $\hat{\mathbf{r}}_B$ (denoting either acceleration, $\hat{\mathbf{a}}_B$, or magnetic field, $\hat{\mathbf{m}}_B$). The sensor EKFs are constructed as three step filters with prediction, outlier mitigation, and correction. The prediction model used is

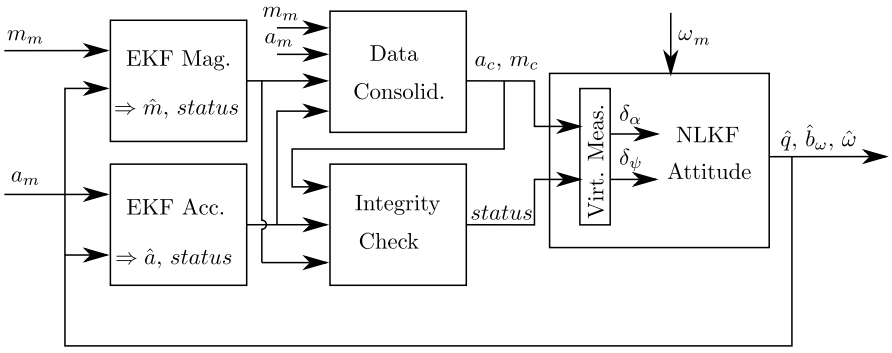

Fig. 1 Fault tolerant attitude estimation architecture overview

$$\hat{\mathbf{r}}_{B,k+1} = \hat{\mathbf{r}}_{B,k} - \left(\hat{\Omega}\hat{\mathbf{r}}_{B,k} + \frac{1}{\tau_r}\left(\hat{\mathbf{r}}_{B,k} - \hat{R}^T \mathbf{r}_{ref}\right)\right)\Delta t, \quad \hat{\Omega} = \left(\omega_m - \hat{\mathbf{b}}_\omega\right)_\times . \tag{9}$$

This model corresponds to a vector measurement that follows the rotation of its reference vector while allowing for transient deviations, e.g. quick accelerations or magnetic perturbations. The time constant τ_r corresponds to presuming that the attitude estimation remains correct during a transient disturbance.

Before the correction step, the norm of the measurement is tested. Since the measurement $\mathbf{r}_{m,k+1}$ is Gaussian, its norm $||\mathbf{r}_{m,k+1}||$ will also be Gaussian with a mean value of $||\mathbf{r}_{ref}||$. We can therefore test the residual $\delta_{||\mathbf{r}_{m,k+1}||} = ||\mathbf{r}_{m,k+1}|| - ||\mathbf{r}_{ref}||$ with a χ^2-test, given a probability of false alarm with the following hypotheses:

$$\begin{aligned} \mathbf{H_0} &: \textit{Measurement norm OK} \Rightarrow r_norm = 0 \\ \mathbf{H_1} &: \textit{Measurement norm NOT OK} \Rightarrow r_norm = 1 \end{aligned} \tag{10}$$

The prediction step is done as per equation (6) with the model 9. The correction step is skipped completely if the status flag *r_norm* is raised. Otherwise, the correction is done as per equation (7), using the measurement equation $\mathbf{r}_{m,k+1} = \mathbf{r}^+_{B,k+1} + \mathbf{w}_{k+1}$. To account for sensor faults that are not seen by the measurement norm, an outlier mitigation is implemented.

4.1.1 Outlier mitigation

A complementary strategy to increase the precision of any Kalman filter is to reject incoherent measurements by testing the innovation. Instead of outright rejection of measurements, it is more cautious to use the measurement but with a decreased gain in order to mitigate its effects.

The innovation ν_{k+1} is calculated for a measurement $\mathbf{r}_{m,k+1}$ as per equation (7) using a mitigated covariance which is built as follows:

Before using a measurement, a check is performed to verify there is an intersection between the prediction and measurement covariances, i.e.

$$\Delta\nu_{k+1,i} \triangleq n_\sigma \left[\sqrt{\left(H_{k+1}\hat{P}^+_{k+1}H^T_{k+1}\right)_{i,i}} + \sqrt{\left(W_{k+1}\right)_{i,i}}\right] \tag{11}$$

where n_σ is the confidence level at which the outlier mitigation starts. The innovation intersection is defined by the test:

$$\Delta\nu_{k+1,i} \underset{\text{Intersection}}{\overset{\text{No intersection}}{\lessgtr}} \nu_{k+1,i} \tag{12}$$

If no intersection is found, we redefine the measurement covariance to include the predicted estimate, by increasing the measurement covariance as:

$$\begin{aligned} W^*_{i,i} &= \left(|\nu|_i - n_\sigma\sqrt{\left(H\hat{P}^+H^T\right)_{i,i}}\right)^2, \quad i,j = \{1,\ldots,\dim(\nu)\} \\ W^*_{i,j} &= 0 \end{aligned} \tag{13}$$

The correction is the done using the covariance W^* instead of W in equation (7). A status flag *r_outlier* is raised if no intersection is detected by the test (12):

$$\begin{aligned} &\mathbf{H_0}: \textit{Measurement intersection} \Rightarrow \textit{r_outlier} = 0 \\ &\mathbf{H_1}: \textit{No measurement intersection} \Rightarrow \textit{r_outlier} = 1 \end{aligned} \tag{14}$$

In addition to the test (12), the outlier flag is also raised if the innovation ν_{k+1} does not pass a whiteness test, i.e:

$$\begin{aligned} &\mathbf{H_0}: \textit{Innovation is white noise} \Rightarrow \textit{r_outlier} = 0 \\ &\mathbf{H_1}: \textit{Innovation is not white noise} \Rightarrow \textit{r_outlier} = 1 \end{aligned} \tag{15}$$

4.1.2 Sensor model integrity

We can check the integrity of the sensor model by projecting the estimate into the inertial frame (assuming $\hat{R}$ is correct) and removing the inertial reference, i.e. $\delta_{\hat{\mathbf{r}}_I} = \hat{R}\hat{\mathbf{r}}_B - \mathbf{r}_{ref}$. As for the measurement norm, this residual is also Gaussian and can be tested with a χ^2 distribution. This test allows to raise a flag concerning the integrity of the sensor model. The hypotheses are in this case:

$$\begin{aligned} &\mathbf{H_0}: \textit{Sensor model integrate} \Rightarrow \textit{r_warn} = 0 \\ &\mathbf{H_1}: \textit{Sensor model not integrate} \Rightarrow \textit{r_warn} = 1 \end{aligned} \tag{16}$$

This test will be sensitive to both divergence in $\hat{R}$ and $\hat{\mathbf{r}}_B$, it can be seen as a general health indicator of the estimation architecture.

In order to better handle transient perturbations, a low level confirmation of 1 second is implemented for all status flags (*r_norm*, *r_outlier*, and *r_warn*). In practice this means trusting the gyroscope during a cool-down period after a perturbation has disappeared (or has drowned in the measurement noise).

4.2 Data consolidation and integrity check blocks: "Data Consolid." and "Integrity check"

The sensor data fed to the attitude estimator is the best available data as per the status flags defined above. In short, if the estimated sensor output is considered compromised then the measurement is used, and vice versa if the sensor model is unreliable. We denote the consolidated measurement $\mathbf{r}_c$. Furthermore, the estimation integrity block assigns the appropriate status to a consolidated sensor data $\mathbf{r}_c$ considering the flags raised by the sensor estimation blocks. The signal status output is called *r_status* and has two possible states:

$$\begin{aligned} r_status = 0 &: \mathbf{r}_c \textit{ NOT OK for attitude update} \\ r_status = 1 &: \mathbf{r}_c \textit{ OK for attitude update} \end{aligned} \tag{17}$$

A summary of the data consolidation and integrity logic is given in Table 1.

Table 1 Sensor data consolidation from status booleans

r_outlier	*r_warn*	*r_norm*	$\mathbf{r}_c =$	*r_status*	Fault description
0	0	0	$\mathbf{r}_m$	1	Nominal, fault-free
1	0	0	$--$	0	Small measurement disturbance
0	1	0	$\mathbf{r}_m$	1	$\hat{R}$ not integrate
1	1	0	$\mathbf{r}_m$	1	$\hat{R}$ or $\hat{\mathbf{r}}_B$ not integrate
0	0	1	$\hat{\mathbf{r}}_B$	1	$\mathbf{r}_m$ not integrate
1	0	1	$--$	0	$\mathbf{r}_m$ or $\hat{\mathbf{r}}_B$ not integrate
0	1	1	$--$	0	$\hat{R}$, $\mathbf{r}_m$, or $\hat{\mathbf{r}}_B$ not integrate
1	1	1	$--$	0	- — — -

The acceleration status is denoted *a_status* and the magnetic field status *m_status*, and the consolidated sensor data $\mathbf{a}_c$ and $\mathbf{m}_c$ respectively.

4.3 Fault tolerant Attitude filter block: "Attitude filter NL-KF"

The role of the attitude filter is to calculate an estimate of the attitude using the consolidated sensor data. The prediction step is calculated at every new gyroscope measurement, and the correction step depends on the status of the vector measurements as calculated by Section 4.2.

4.3.1 State prediction

The attitude filter is based on the quaternion kinematics in equation (4), we also estimate the gyroscope bias $\mathbf{b}_\omega$ using a saturated bias model. This yields the discrete state prediction:

$$\begin{aligned} \hat{\mathbf{q}}_{k+1}^{+} &= \hat{\mathbf{q}}_k + \frac{1}{2}\Omega\left(\omega_m - \hat{\mathbf{b}}_{\omega,k}\right)\Delta t\,\hat{\mathbf{q}}_k \\ \hat{\mathbf{b}}_{\omega,k+1}^{+} &= \hat{\mathbf{b}}_{\omega,k} - k_{AW}\left(\hat{\mathbf{b}}_{\omega,k} - \mathrm{sat}\left(\hat{\mathbf{b}}_{\omega,k}, \bar{b}_\omega\right)\right)\Delta t \end{aligned} \tag{18}$$

where $k_{AW} \in [0,\,1]$ is the bias anti-windup gain and $\bar{b}_\omega$ the maximum admissible bias. The covariance is propagated as per equation 6, with the matrices F_k and Q_k defined by:

$$\begin{aligned} F_k &= \begin{bmatrix} I + \frac{1}{2}\Omega\left(\omega_m - \hat{\mathbf{b}}_{\omega,k}\right)\Delta t\hat{\mathbf{q}}_k & \frac{\partial \hat{\mathbf{q}}_{k+1}^{+}}{\partial \hat{\mathbf{b}}_{\omega,k}} \\ 0 & \left[1 - \frac{\Delta t}{\tau_b}\left(1 - N_{eq}\right)\right]^2 \end{bmatrix} \\ Q_k &= \begin{bmatrix} \left(\frac{\partial \hat{\mathbf{q}}_{k+1}^{+}}{\partial \omega_m}\right)\begin{bmatrix} 0 & 0 \\ 0 & V_\omega \end{bmatrix}\left(\frac{\partial \hat{\mathbf{q}}_{k+1}^{+}}{\partial \omega_m}\right)^T & 0 \\ 0 & \Delta t\, V_{b_\omega} \end{bmatrix} \end{aligned} \tag{19}$$

The covariance matrices V_ω and V_{b_ω} are diagonal and given by the noise power and rate random walk of the gyroscope respectively. The gain $N_{eq} \in [0,\,1]$ is called the *equivalent stochastic gain* and results from a stochastic linearisation of the bias saturation. This gives a behaviour similar to an unscented Kalman filter. The correction step is divided into a correction of the inclination and of the heading estimation performed sequentially.

4.3.2 State correction

The additive update of the EKF is unfit for quaternion update since the correction loses its physical meaning. An alternative is to use a multiplicative extended Kalman filter (MEKF) where the corrected quaternion remains a rotation [17]. We can generalise the MEKF correction as a nonlinear function of the predicted quaternion and the measurements, i.e:

$$\hat{\mathbf{q}}_{k+1} = \mathbf{g}\left(\hat{\mathbf{q}}^{+}_{k+1}, \mathbf{r}_{c,k+1}\right) \tag{20}$$

The associated covariance update is then:

$$\begin{aligned} \hat{P}_{k+1} &= G_{\hat{\mathbf{x}}^{+}_{k+1}} \hat{P}^{+}_{k+1} G^{T}_{\hat{\mathbf{x}}^{+}_{k+1}} + G_{\mathbf{y}_{k+1}} W_{k+1} G^{T}_{\mathbf{y}_{k+1}} \\ \text{with} \quad G_{\hat{\mathbf{x}}^{+}_{k+1}} &= \frac{\partial \mathbf{g}}{\partial \hat{\mathbf{x}}^{+}_{k+1}}, \quad G_{\mathbf{y}_{k+1}} = \frac{\partial \mathbf{g}}{\partial \mathbf{r}_{c,k+1}} . \end{aligned} \tag{21}$$

We note that this covariance update using Joseph's form gives no guarantee of a decreased covariance, although it preserves its positive semi-definite form. A filter using this kind of correction should not be classified as an EKF, but rather as a nonlinear Kalman filter (NL-KF), since its gain does not depend on the linearisation of the measurement equation.

We also note that the bias must be updated separately since the correlation due to the Kalman gain is artificially set to zero when correcting the quaternion with (20).

The state correction of the attitude filter is conditionalised by the status variables *a_status* and *m_status* calculated by the "Integrity check" block. The state correction is done as per the following sequential procedure (the covariance is updated accordingly at each step using (21)):

– Set the corrected state to the predicted state: $\hat{\mathbf{q}}_{k+1} = \hat{\mathbf{q}}^{+}_{k+1}$, $\hat{\mathbf{b}}_{k+1} = \hat{\mathbf{b}}^{+}_{k+1}$
– if $a_status = 1$: Inclination and bias correction $(b_{\omega_x}, b_{\omega_y})$ with a_c
  • $\hat{\mathbf{q}}_{k+1} = \hat{\mathbf{q}}_{k+1} \otimes \delta\mathbf{q}_{(\alpha,\hat{\mathbf{u}})}\left(\hat{\mathbf{q}}_{k+1}, a_c, k_\alpha\right)$
  • $\begin{pmatrix} \hat{b}_{\omega,x} \\ \hat{b}_{\omega,y} \end{pmatrix}_{k+1} = \begin{pmatrix} \hat{b}_{\omega,x} \\ \hat{b}_{\omega,y} \end{pmatrix}_{k+1} + \begin{pmatrix} k_p\, u_1 \\ k_q\, u_2 \end{pmatrix} \delta\alpha$
– if $m_status = 1$: Heading and bias correction (b_{ω_z}) with m_c
  • $\hat{\mathbf{q}}_{k+1} = \hat{\mathbf{q}}_{k+1} \otimes \delta\mathbf{q}_{(\psi,\mathbf{e}_3)}\left(\hat{\mathbf{q}}_{k+1}, m_c, k_\psi\right)$
  • $\hat{b}_{\omega,z,k+1} = \hat{b}_{\omega,z,k+1} + k_r\, \delta\psi$

The gains k_p, k_q, k_r, k_α, and k_ψ are all $\in [0, 1]$ and are chosen to fix a first order response time. The procedures for calculating $\delta\alpha$, $\delta\psi$, $\delta\mathbf{q}_{(\psi,\mathbf{e}_3)}$, and $\delta\mathbf{q}_{(\alpha,\hat{\mathbf{u}})}$ are given by the following calculations:

Inclination correction:

Inclination axis

$$\hat{\mathbf{u}} \triangleq \mathrm{Ker}\left(\begin{bmatrix}\mathbf{e}_3^T\hat{R}\\ \mathbf{e}_3^T\end{bmatrix}\right) = (u_1, u_2, 0)^T$$

Estimated inclination

$$\cos\hat{\alpha} = \mathbf{e}_3^T\hat{R}^T\mathbf{e}_3$$

$$\sin\hat{\alpha} = -\hat{\mathbf{u}}^T\left(\mathbf{e}_3\times\hat{R}^T\mathbf{e}_3\right)$$

$$R_{(\hat{\alpha},\hat{\mathbf{u}})} = I + \sin\hat{\alpha}\,\hat{\mathbf{u}}_\times + (1-\cos\hat{\alpha})\,\hat{\mathbf{u}}_\times^2$$

Inclination error measurement

$$\mathbf{y}_m \triangleq R_{\hat{\alpha},\hat{\mathbf{u}}}\frac{\mathbf{a}_c}{[||\mathbf{a}_c||}$$

$$\delta\alpha = \mathrm{atan2}\left(\hat{\mathbf{u}}^T\left(\mathbf{e}_3\times\mathbf{y}_m\right), \mathbf{e}_3^T\mathbf{y}_m\right)$$

Inclination correction angle

$$\Delta\alpha = k_\alpha\delta\alpha$$

Correction quaternion

$$\delta\mathbf{q}_{(\alpha,\hat{\mathbf{u}})} = (\cos(\Delta\alpha/2), \hat{\mathbf{u}}\sin(\Delta\alpha/2))^T$$

Heading correction:

Magnetic error vector

$$y_1 = \mathbf{m}_{ref}^T\left(\hat{R}\mathbf{m}_B\times\mathbf{e}_3\right)$$

$$y_2 = \left(\mathbf{m}_{ref}\times\mathbf{e}_3\right)^T\left(\hat{R}\mathbf{m}_B\times\mathbf{e}_3\right)$$

$$\mathbf{y} \triangleq (y_1, y_2)$$

Heading error angle

$$s = \frac{y_1}{||\mathbf{y}||} = \sin(\delta\psi)$$

$$c = \frac{y_2}{||\mathbf{y}||} = \cos(\delta\psi)$$

$$\delta\psi = \mathrm{atan2}(s, c)$$

Heading correction angle

$$\Delta\psi = k_\psi\,\delta\psi$$

Correction quaternion

$$\hat{\delta\mathbf{q}}_\psi = (\cos(\Delta\psi/2), \mathbf{e}_3\sin(\Delta\psi/2))^T$$

The rotation vector $\hat{\mathbf{u}}$ is by definition $\perp \mathbf{e}_3$, therefore the inclination correction will not impact the heading correction and vice versa.

5 Architecture tuning

The attitude filter was configured to have a (3τ) response time of $\sim$10s in roll and pitch, and $\sim$10s in yaw. The gyroscope bias response times were set to 100s , the bias saturation was set to $0.01\mathrm{rad/s}$, and the anti-windup gain was tuned to $0.025\mathrm{s}\cdot$ The sensor performance models' response times were set to 10s in both the acceleration and magnetic field estimators.

The statistical tests of the fault detection were all set to a false alarm rate corresponding to 3σ. The false alarm rate practically means a trade off between trusting the gyroscope or the vector measurements due to the gated attitude corrections, much like the measurement covariances in a standard EKF.

6 Experimental results

A series of flight tests with a MikroKopter MK7 quadrotor [18] drone, carrying a Pixhawk 4 module [19] providing accelerometer, gyroscope, and magnetometer measurements, plus an on-board attitude estimation. A ground truth of the quadrotor attitude was obtained via an optical tracking system [20].

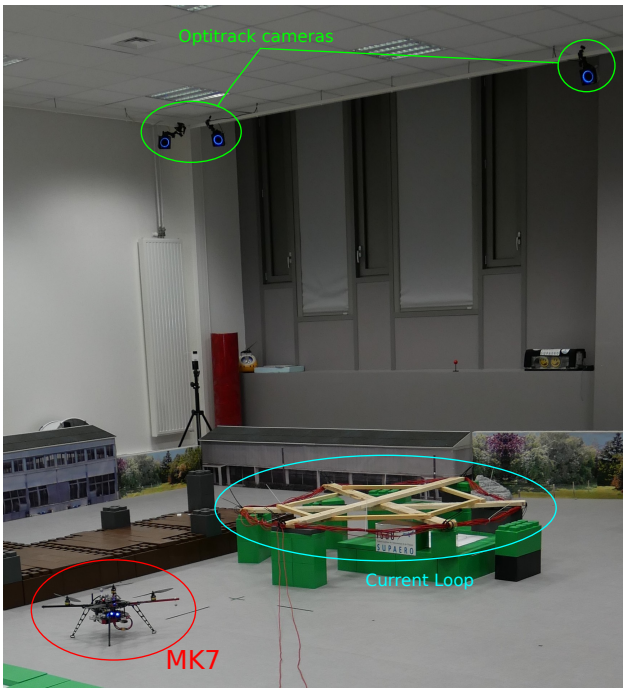

Fig. 2 The experimental set-up with the quadrotor, the current loop, and the optical tracking system visible.

In order to obtain controllable magnetic disturbances, a home made current loop fixed to a wooden armature was placed in the flight arena. We can then easily activate or deactivate a known magnetic disturbance using this current loop. In the following scenarios, a current of 15A was run through the loop. The loop itself was a circle of $\approx$ 2m in diameter consisting of 2.5mm^2 copper wire run 15 rounds around the armature. This gave a maximum field strength of $\approx$ 2G , as can be seen in the magnetometer readings. Three different trajectories were tested to highlight the different problems and solutions.

1. Cross-trajectory with high accelerations, no magnetic disturbance present.
2. Slow horizontal and vertical approaches into the magnetic disturbance followed by slow distancing.
3. Cross trajectory with high accelerations in and out of the magnetic disturbance.

Three filters are shown for each scenario: the onboard PX4 estimator (PX4); the decoupled nonlinear attitude filter in section 4.3 (DEC-KF); the entire fault tolerant architecture (FT-KF) in section 4. To avoid long transients in the replayed data, the gyroscope bias estimates were initialised with the slope of the error between the purely integrated gyroscopes and the attitude given by the tracking system.

The onboard estimation was calculated at 250Hz, but due to packet-losses when saving the data, the recordings of the IMU and magnetometer did not have a consistent frequency. The average sampling frequency of the replayed data was $\sim$ 190Hz for the IMU (gyroscope and accelerometer) and $\sim$ 90Hz for the magnetometer.

6.1 Cross-trajectory

Given the inertial measurements in Figs. 3 and 4, Fig. 5 shows the inclination- and heading error and Table 4 the associated statistics. The integrity booleans are shown in Fig. 6.

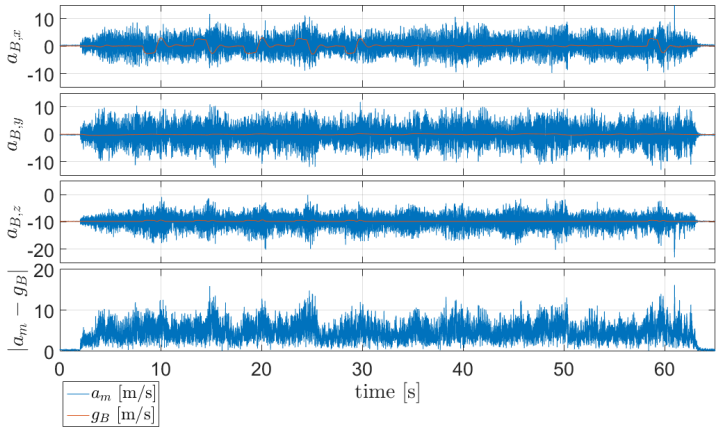

Fig. 3 Cross trajectory: Accelerometer ($\mathbf{a}_m$) vs gravity in body frame (g_B)

Table 2 Cross trajectory: Estimation error statistics

	max(ε_ψ)	mean(ε_ψ)	std(ε_ψ)	max(ε_α)	mean(ε_α)	std(ε_α)
PX4	14.18	9.73	3.67	5.00	2.89	0.39
NL-KF	16.16	8.98	4.04	8.06	2.34	1.35
FT-KF	18.28	10.22	4.43	7.67	2.27	1.34

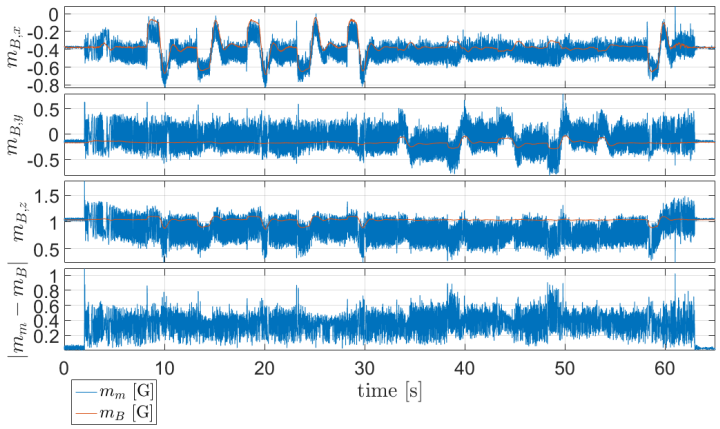

Fig. 4 Cross trajectory: Magnetometer ($\mathbf{m}_m$) vs magnetic reference in body frame ($\mathbf{m}_B$)

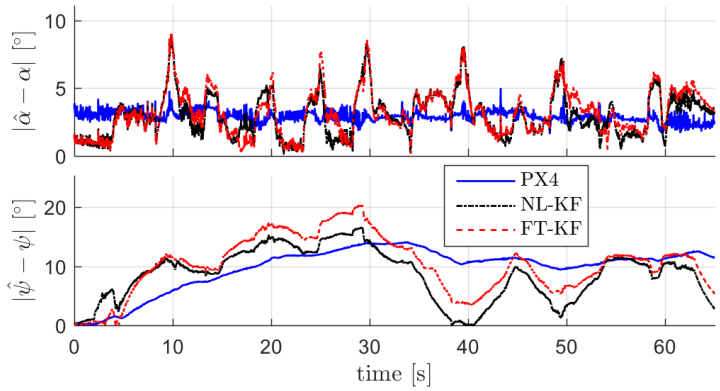

Fig. 5 Cross trajectory: Inclination (α) and heading (ψ) errors

In this scenario, mainly transverse accelerations disturb the IMU. In the integrity booleans in Fig. 6 we clearly see the detection of the acceleration outliers (*a_outlier*). The few magnetic disturbance detections (*m_outlier*) are likely due to the inhomogeneity of the magnetic field in the flight arena (armed concrete floor, etc.). The statistics show no major difference in the three estimators apart from the higher covariance in inclination due to a lower sampling rate in the replayed data compared to the onboard estimation.

6.2 Slow approach of magnetic disturbance

Given the inertial measurements in Figs. 7 and 8, Fig. 9 shows the inclination- and heading error, Fig. 10 the integrity booleans, and Table 3 the associated statistics.

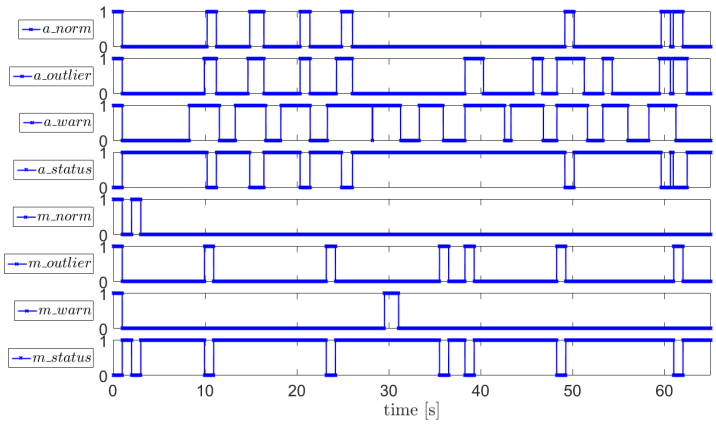

Fig. 6 Cross trajectory: Integrity booleans

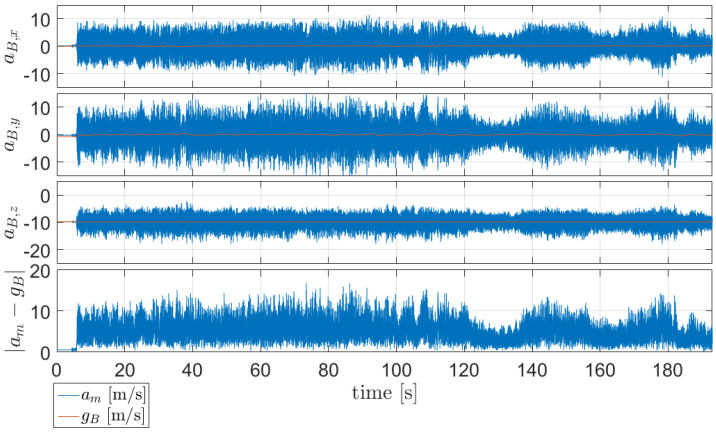

Fig. 7 Slow approach trajectory with magnetic disturbance: Accelerometer ($\mathbf{a}_m$) vs gravity in body frame (g_B)

Table 3 Slow approach trajectory: Estimation error statistics

	max(ε_ψ)	mean(ε_ψ)	std(ε_ψ)	max(ε_α)	mean(ε_α)	std(ε_α)
PX4	79.40	17.76	22.77	3.40	2.01	0.55
NL-KF	154.31	49.14	54.21	6.71	2.24	1.28
FT-KF	9.92	2.59	2.69	6.73	2.24	1.29

The FT-KF manages the magnetic perturbations well. In comparison to the PX4 which works on measurement rejection through innovation testing only, the FT-KF manages to reject even the disturbance between $\sim$ 120s and $\sim$ 180s, and reconverge as it disappears. We also note in this case the exponential convergence of the DEC-

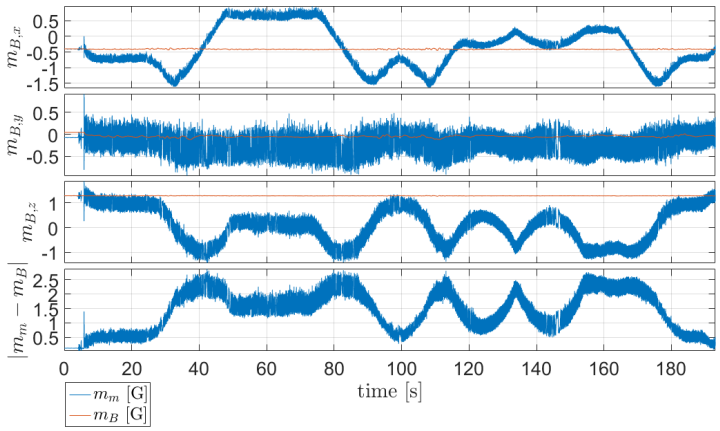

Fig. 8 Slow approach trajectory with magnetic disturbance: Magnetometer ($\mathbf{m}_m$) vs magnetic reference in body frame ($\mathbf{m}_B$)

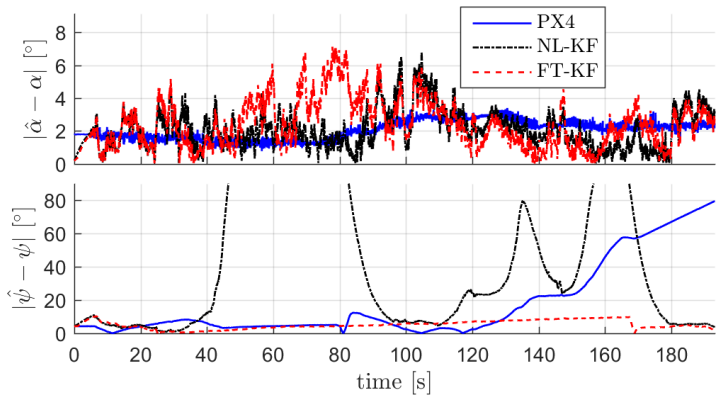

Fig. 9 Slow approach trajectory with magnetic disturbance: Inclination (α) and heading (ψ) errors

KF in yaw. The NL-KF works well in α since only $\mathbf{a}_m$ is used to correct the inclination. It does not work in the heading estimation since it uses a measurement ($\mathbf{m}_m$) which is heavily biased (and no detector is used, as for the FT-KF). We also note the reconvergence as soon as the disturbance disappears (with the chosen response time of 10 seconds). The slight increase in heading error for the FT-KF around 170s is due to the missed outlier detection seen in Fig. 10. This scenario also shows a bunch of detections in the accelerometer data, this corresponds to the peaks in $\mathbf{a}_{m,y}$ between 30-120s and seems to be due to ground and wall effects.

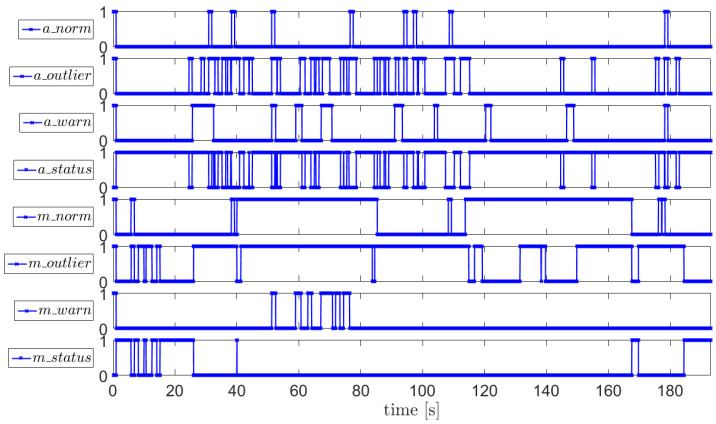

Fig. 10 Slow approach trajectory with magnetic disturbance: Integrity booleans

6.3 Cross-trajectory with magnetic disturbance

Given the inertial measurements in Figs. 11 and 12, Fig. 13 shows the inclination- and heading error, Fig. 14 the integrity booleans, and Table 4 the associated statistics.

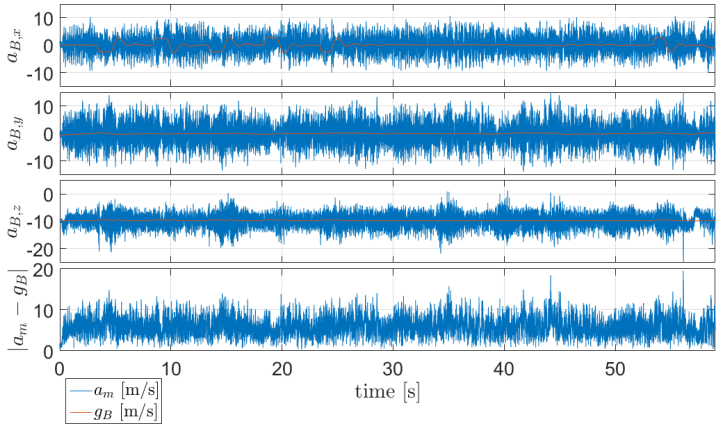

Fig. 11 Cross trajectory with magnetic disturbance: Accelerometer ($\mathbf{a}_m$) vs gravity in body frame (g_B)

In this case we see that the FT-KF deviates less than the PX4 in yaw, although the error in both cases remains modest. This is likely due to the measurement rejection implemented in the PX4 which works well for transient disturbances. We clearly see the interest of the detection and rejection stage of the fault tolerant FT-KF as compared to the decoupled-only NL-KF. Compared to the PX4, the precision in

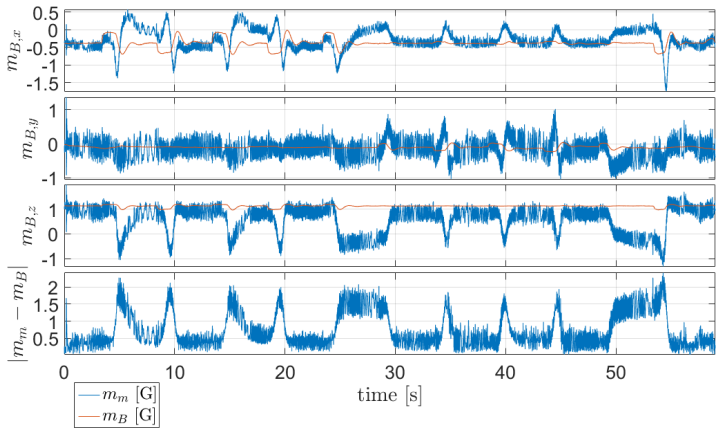

Fig. 12 Cross trajectory with magnetic disturbance: Magnetometer ($\mathbf{m}_m$) vs magnetic reference in body frame ($\mathbf{m}_B$)

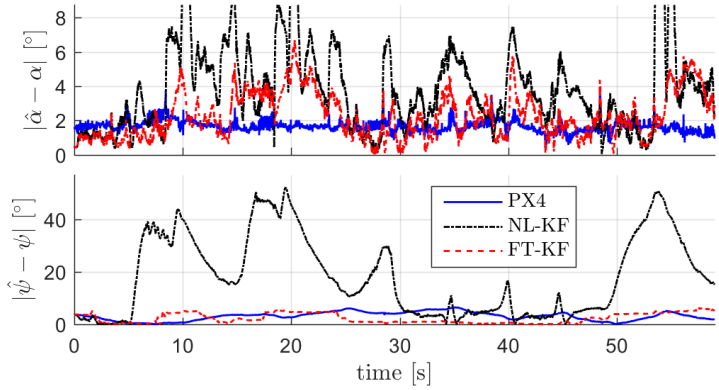

Fig. 13 Cross trajectory with magnetic disturbance: Error angles for cross-trajectory with magnetic disturbance

Table 4 Cross trajectory with magnetic disturbance: Estimation error statistics

	$\max(\varepsilon_\psi)$	$\text{mean}(\varepsilon_\psi)$	$\text{std}(\varepsilon_\psi)$	$\max(\varepsilon_\alpha)$	$\text{mean}(\varepsilon_\alpha)$	$\text{std}(\varepsilon_\alpha)$
PX4	6.45	3.08	1.64	3.74	1.65	0.33
NL-KF	50.72	17.22	14.36	8.16	2.31	1.36
FT-KF	5.03	2.11	0.78	4.98	2.18	0.86

inclination is worse for the FT-KF and DEC-KF due to the lower sampling frequency and possibly missing data during the dynamic parts.

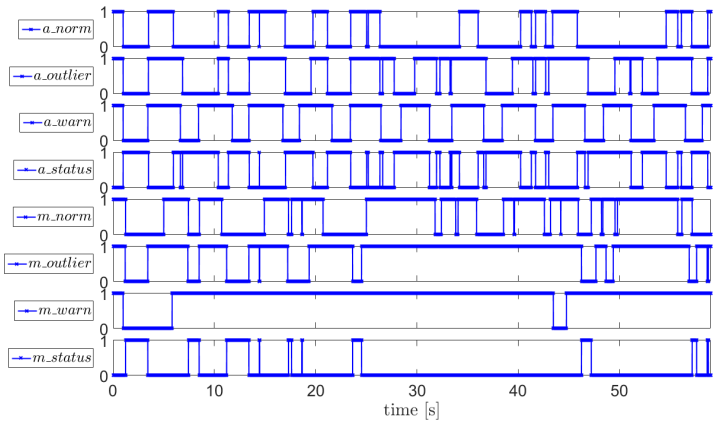

Fig. 14 Cross trajectory with magnetic disturbance: Integrity booleans

7 Conclusion

We have presented a fault tolerant attitude estimation architecture for handling large inertial accelerations and time varying magnetic disturbances. Experimental results using low-cost MEMS sensors confirm the presumed decoupling and disturbance rejection properties.

The developed estimator consists of two key elements:

- A prediction procedure that assures a realistic estimation of gyroscope biases and their associated uncertainties.
- A correction procedure that assures a decoupling of the information, given by the accelerometer and the magnetometer, used to correct the inclination and the heading. This decoupling also allows sensor faults to be easily localised.

Furthermore we show the interest of a detection stage to assure the integrity of the heading when subject to magnetic disturbances. The equivalent detection for the inclination is arguably less important, but this is probably due to the limited high accelerations we have tested because of the limited test area. Same tests in an open space allowing higher accelerations disturbances would probably be more demonstrative. We see that the proposed attitude filter (NL-KF) re-converges even at large attitude errors. This is seemingly not the case for the EKF based PX4.

The architecture presented here uses a simple one-step χ^2-test for fault detection. We see that this test is not powerful enough for slowly growing or low amplitude faults. The detection stage could be improved by using more sophisticated methods such as (χ^2-)CUSUM or GLR tests ([21], [22]). Another axis of improvement would be to adapt the measurement covariances to decrease the rate of false alarm while keeping the rate of missed detections.

References

1. G. Alcalay, C. Seren, G. Hardier, M. Delporte, and P. Goupil, "An adaptive extended kalman filter for monitoring and estimating key aircraft flight parameters," *IFAC-PapersOnLine*, vol. 51, no. 24, pp. 620–627, 2018.
2. G. Allibert, R. Mahony, and M. Bangura, "Velocity aided attitude estimation for aerial robotic vehicles using latent rotation scaling," in *IEEE ICRA*. IEEE, 2016, pp. 1538–1543.
3. M.-D. Hua, "Attitude estimation for accelerated vehicles using gps/ins measurements," *Control Engineering Practice*, vol. 18, no. 7, pp. 723–732, 2010.
4. S. Bonnable, P. Martin, and E. Salaün, "Invariant extended kalman filter: theory and application to a velocity-aided attitude estimation problem," in *Proceedings of the 48th IEEE Conference on Decision and Control*. IEEE, 2009, pp. 1297–1304.
5. A. Roberts and A. Tayebi, "On the attitude estimation of accelerating rigid-bodies using gps and imu measurements," in *IEEE Conference on Decision and Control*. IEEE, 2011, pp. 8088–8093.
6. T. Hamel and R. Mahony, "Attitude estimation on so [3] based on direct inertial measurements," in *ICRA*. IEEE, 2006, pp. 2170–2175.
7. C.-I. Chesneau, M. Hillion, J.-F. Hullo, G. Thibault, and C. Prieur, "Improving magneto-inertial attitude and position estimation by means of a magnetic heading observer," in *International Conference on Indoor Positioning and Indoor Navigation*. IEEE, 2017, pp. 1–8.
8. R. Mahony, T. Hamel, and J.-M. Pflimlin, "Nonlinear complementary filters on the special orthogonal group," *IEEE TAC*, vol. 53, 2008.
9. J.-P. Condomines, C. Seren, and G. Hattenberger, "Invariant unscented kalman filter with application to attitude estimation," in *56th Annual Conference on Decision and Control*. IEEE, 2017, pp. 2783–2788.
10. H. G. De Marina, F. J. Pereda, J. M. Giron-Sierra, and F. Espinosa, "Uav attitude estimation using unscented kalman filter and triad," *IEEE Transactions on Industrial Electronics*, vol. 59, no. 11, pp. 4465–4474, 2012.
11. W. Li and J. Wang, "Effective adaptive kalman filter for mems-imu/magnetometers integrated attitude and heading reference systems," *The Journal of Navigation*, vol. 66, no. 1, pp. 99–113, 2013.
12. T. A. Johansen and T. I. Fossen, "The exogenous kalman filter (xkf)," *International Journal of Control*, vol. 90, no. 2, pp. 161–167, 2017.
13. P. Martin and I. Sarras, "A global observer for attitude and gyro biases from vector measurements," *IFAC-PapersOnLine*, vol. 50, 2017.
14. L. A. McGee and S. F. Schmidt, "Discovery of the kalman filter as a practical tool for aerospace and industry," *NASA Technical Memorandum 86847*, 1985.
15. P. Martin and E. Salaun, "Invariant observers for attitude and heading estimation from low-cost inertial and magnetic sensors," in *Decision and Control, 2007 46th IEEE Conference on*. IEEE, 2007, pp. 1039–1045.
16. M.-D. Hua, K. Rudin, G. Ducard, T. Hamel, R. Mahony *et al.*, "Nonlinear attitude estimation with measurement decoupling and anti-windup gyro-bias compensation," in *IFAC World Congress*, 2011, pp. 2972–2978.
17. F. L. Markley, "Multiplicative vs. additive filtering for spacecraft attitude determination," *Dynamics and Control of Systems and Structures in Space*, no. 467-474, 2004.
18. "Mikrokopter," http://www.mikrokopter.de/en/home, accessed: 2018-10-19.
19. "Px4 tutorial," https://dev.px4.io/en/tutorials/tuning_the_ecl_ekf.html, accessed: 2018-10-19.
20. "Optitrack - motion capture systems," http://optitrack.com, accessed: 2018-08-17.
21. F. Gustafsson, *Adaptive filtering and change detection*. Citeseer, 2000, vol. 1.
22. G. Öman Lundin, P. Mouyon, and A. Manecy, "A glr algorithm for multiple consecutive measurement bias estimation," in *Research, Education, and Development for Unmanned Aerial Systems*. IEEE, 2017.